

## 2D numerical comparison of trailing edge flaps - UpWind WP1B3

Thomas Buhl<sup>1</sup>, Peter B. Andersen<sup>1</sup> and Thanasis K. Barlas<sup>2</sup>

<sup>1</sup>Risø National Laboratory

<sup>2</sup>DUWIND – Delft Technical University

Risø-R-1628(EN)

**Author:** Thomas Buhl  
**Title:** 2D numerical comparison of trailing edge flaps  
**Department:** Department of wind energy

**Risø-R-1628(EN)**  
**November 2007**

**Abstract :**

This report covers the investigations and comparisons of trailing edge flaps carried out by Delft and Risø. The work is a part of the W1B3 work package of the UpWind EU-project. This report covers only 2D test cases with simple control of the trailing edge flap with the objective of keeping  $C_L$  constant. The 5MW UpWind reference turbine is used for the calculations. The section in 75% radius is investigated for three different cases; 1) a wind step from 10m/s to 11m/s, 2) a wind “gust” from 10 m/s to 14m/s in 1 second and followed by 10m/s, 3) finally a turbulent wind series is simulated, and the performance of the flaps is investigated. The two different codes from Delft and Risø are compared in the mentioned cases.

**ISSN 0106-2840**  
**ISBN 978-87-550-3647-5**

**Contract no.:**

**Group's own reg. no.:**  
1110051-01

**Sponsorship:**

**Cover :**

**Pages:21**  
**Tables:6**  
**References:5**

Information Service Department  
Risø National Laboratory  
Technical University of Denmark  
P.O.Box 49  
DK-4000 Roskilde  
Denmark  
Telephone +45 46774004  
[bibl@risoe.dk](mailto:bibl@risoe.dk)  
Fax +45 46774013  
[www.risoe.dk](http://www.risoe.dk)

# Contents

## **Preface 4**

### **1 Risø contribution 5**

1.1 Description of model 5

1.2 Numerical results 6

1.2.1 Wind step 6

1.2.2 Wind gust 8

1.2.3 Turbulent wind 10

### **2 DUWIND contribution 13**

2.1 Description of model 13

2.2 Description of investigated cases 13

2.3 Results 14

2.3.1 Wind step 14

2.3.2 Square wind input 15

2.3.3 Turbulent wind input 17

### **3 References 20**

## Preface

This report covers the investigations and comparisons of trailing edge flaps carried out by Delft and Risø. The work is a part of the WIB3 work package of the UpWind EU-project. This report covers only 2D test cases with simple control of the trailing edge flap with the objective of keeping  $C_L$  constant. The 5MW UpWind reference turbine is used for the calculations. The section in 75% radius is investigated for three different cases; 1) a wind step from 10m/s to 11m/s, 2) a wind “gust” from 10 m/s to 14m/s in 1 second and followed by 10m/s, 3) finally a turbulent wind series is simulated, and the performance of the flaps is investigated. The two different codes from Delft and Risø are compared in the mentioned cases.

# 1 Risø contribution

## 1.1 Description of model

The model consists of two parts; an inviscid and a viscous part. In the inviscid part the airfoil is represented by its camberline with a mounted adaptive trailing edge geometry (ATEG) also represented by a camberline. The influence from the shed vorticity in the wake is described by a series of time-lags as used by Hansen et al. [2] and Gaunaa [1], in which the time-lag is approximated using an indicial function first outlined by Von Karman et al [3], making the practical calculation of the aerodynamic response numerically very efficient by use of Duhamel superposition. In the viscous part of the model the dynamic behavior of the trailing edge (TE) separation is likewise modeled using an assumed time-lag between pressure distribution and lift and a time-lag for the separation point in the dynamic boundary layer. Using the same conditions as specified by Hansen et al. [2] the TE separation is considered under stalled conditions.

Based on the work of Gaunaa [1], the lift, drag and moment can be found for an airfoil using a series of mode shapes which model an unsteady camberline. A single mode shape can be used to model the camberline of an ATEG undergoing unsteady deformations. The model is based on the Beddoes-Leishman (B-L) model which originally deals with both LE vortex shedding and TE separation; however, LE eddy separation is not included in the model. Two state variables in the B-L model are used to describe the dynamic behavior of the TE separation. The separation is related to the pressure distribution over the airfoil, and the pressure is related to the lift on the airfoil; for a given lift there is a certain pressure distribution with a certain separation point. In Figure 1 the fully separated and fully attached lift is shown as a function of AOA and ATEG deflection. The unsteady drag is bounded to variations about a static drag curve provided as input to the model. The drag consists of three parts; *Induced drag*, *viscous drag* and *ATEG contribution to drag* modeled as a change in AOA offset similar to the dynamic lift. A description of the *induced drag* is provided by Hansen et al. [2]. The *viscous drag* is either calculated using CFD or measured in a wind tunnel. The unsteady TE separation affects the moment through the traveling of the pressure center due to separation. However as for the drag, the present model binds the unsteady moment to variations about the static moment curve provided as input.

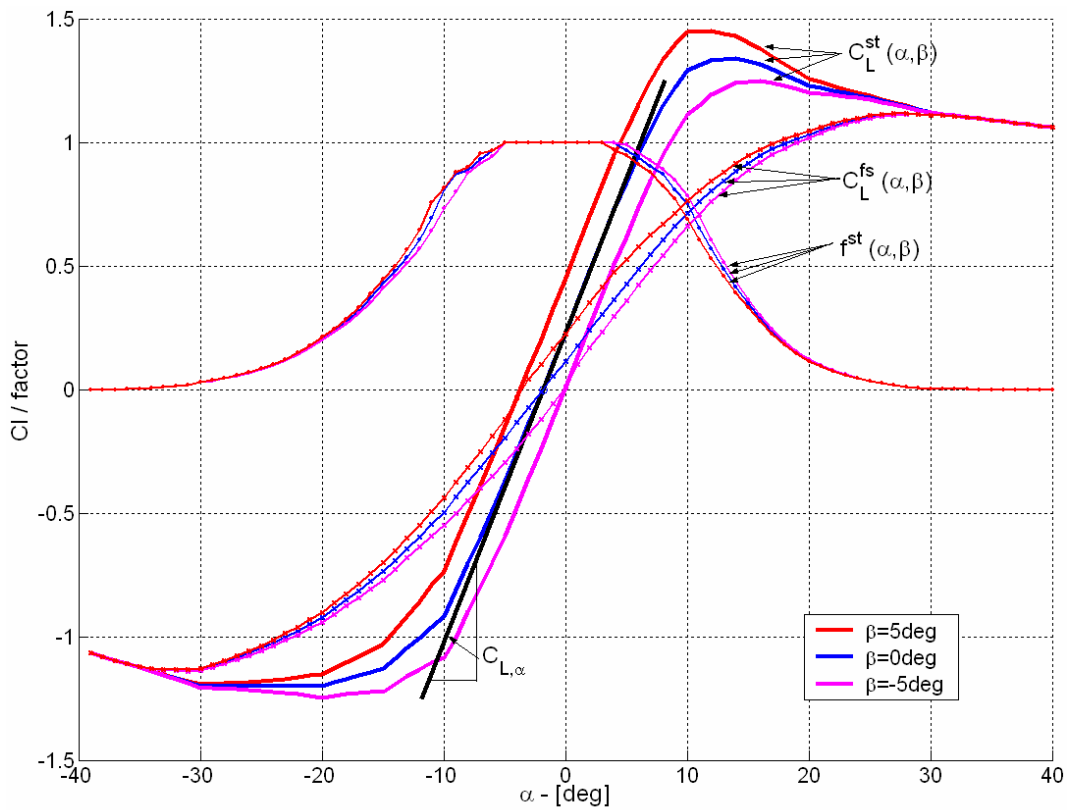


Figure 1 Example of a static lift curves for ATEG deflection for  $\beta = -5, 0$  and  $5$  degree.

## 1.2 Numerical results

In the following section three different test cases are investigated. In all cases the profile section investigated is the section in 75% radius of the UpWind reference turbine. The chord is 2.85 m and it is rotating with 60m/s. The flap deflection angle is limited to +/- 10 deg. In all cases a PID controller is used and tuned with the Ziegler-Nichols' method. The aim of the control is to keep  $C_L$  constant. It is assumed that the flap has no mass and there is no time lag in the system.

### 1.2.1 Wind step

The first test case is a wind step where the wind speed changes from 10 m/s to 11 m/s at 10 seconds in a 20 second time series. In Figure 2 the wind series and the response is shown for the wind step case without control. In Figure 3 the response is shown for the controlled case. The reduction in the standard deviation of  $C_L$  is 97% as shown in Table 2. As a further benefit is that the standard deviation of  $C_D$  is reduced with 73.8%, however,  $C_M$  has increased with 302%.

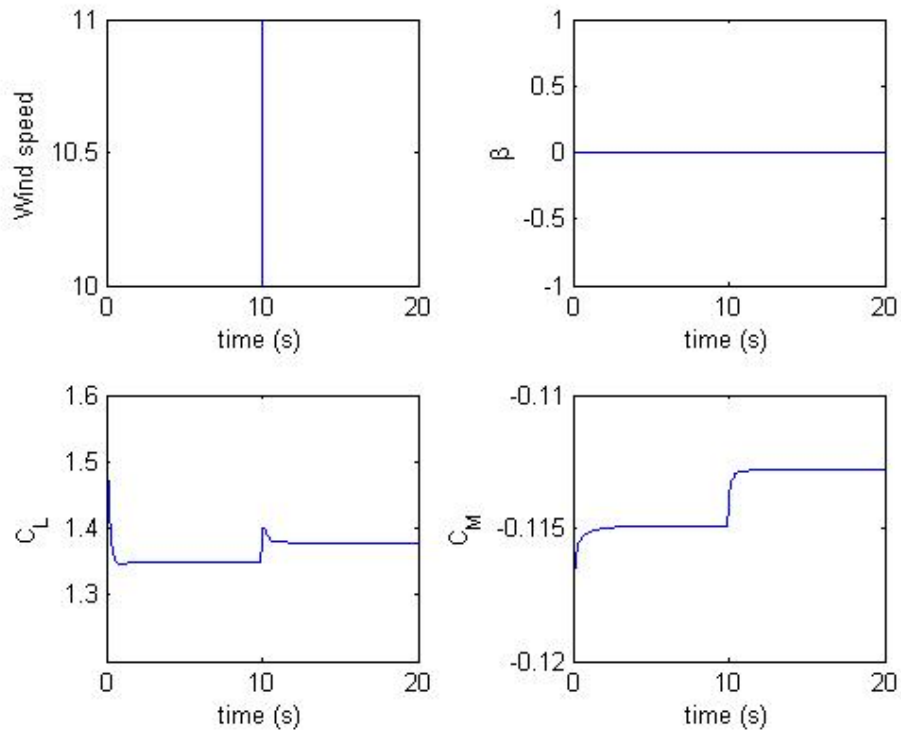


Figure 2 The wind step is shown in the upper left graph. There is no active control as seen in the upper right graph. The lower left graph shows  $C_L$  response and the lower right graph shows the  $C_M$  response.

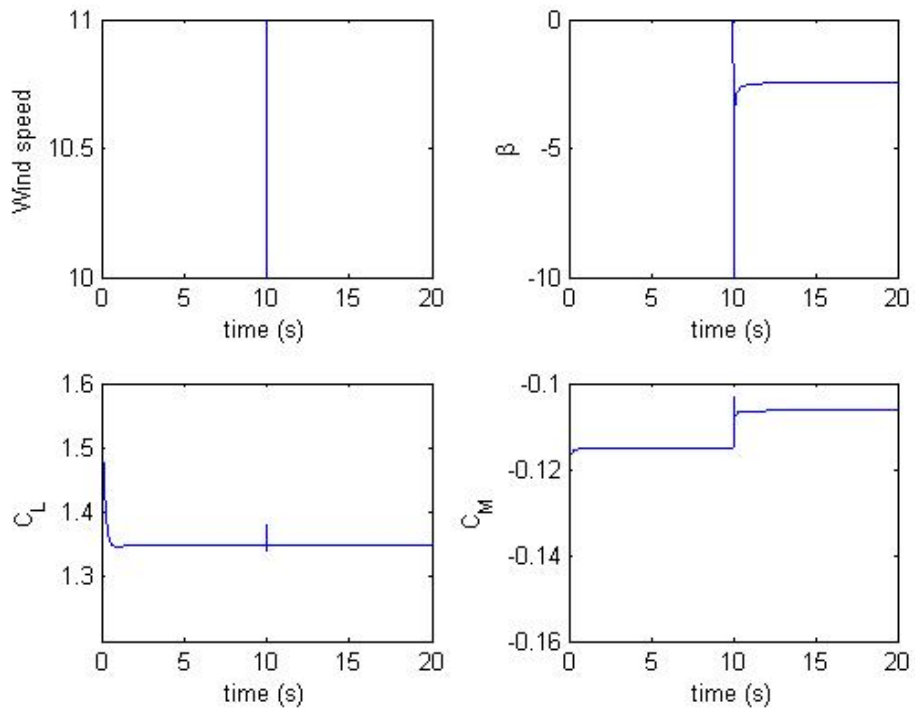


Figure 3 The wind step is shown in the upper left graph. The control is active and the flap deflection is seen in the upper right graph. The lower left graph shows  $C_L$  response and the lower right graph shows the  $C_M$  response.

Table 1 Wind step results. “No con” denotes where the control is inactive, while “Con” denotes where the control is active.

	Std		Mean		Min		Max	
	No con	Con	No con	Con	No con	Con	No con	Con
$C_L$	0.0141	$4.29 \cdot 10^{-4}$	1.3697	1.3501	1.3501	1.3417	1.4014	1.3800
$C_D$	0.0042	0.0011	0.0223	0.0171	0.0164	0.0164	0.0320	0.0320
$C_M$	$9.95 \cdot 10^{-4}$	0.0040	-0.1128	-0.1092	-0.1149	-0.1149	-0.1135	-0.1032

Table 2 Wind step results shown in percentage. Increases (shown in negative numbers) and decreases in  $C_L$ ,  $C_D$  and  $C_M$ .

	Diff Std	Diff Mean	Diff Min	Diff Max
$C_L$	97.0%	1.43%	0.62%	1.53%
$C_D$	73.8%	23.3%	0.0%	0.0%
$C_M$	-302%	3.19%	0.0%	9.07%

### 1.2.2 Wind gust

In this section an idealized wind gust case is analyzed. The wind series starts with 10 m/s and at 10 s the wind changes instantaneously to 14 m/s and changes back to 10 m/s at 11 s as shown in Figure 4. Since the pitch angle is kept constant, the flap angle reaches the maximum flap deflection immediately as seen in Figure 5. From Table 3 it can be seen that the standard deviation of  $C_L$  is decreased by 55.7%. As the previous case the standard deviation of  $C_M$  has increased.

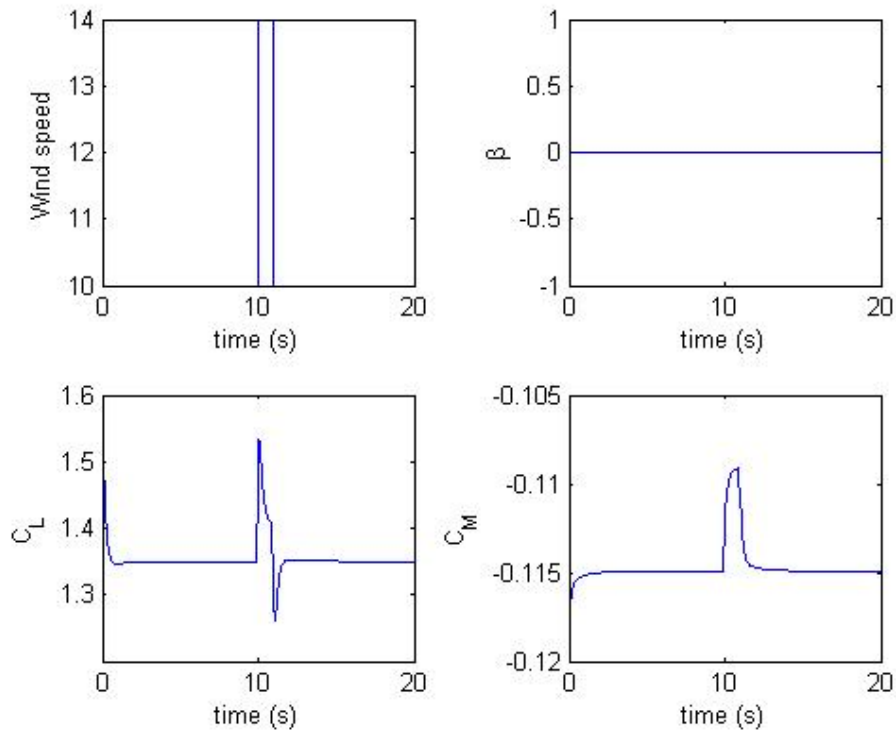


Figure 4 The wind gust is shown in the upper left graph. There is no active control as seen in the upper right graph. The lower left graph shows  $C_L$  response and the lower right graph shows the  $C_M$  response.

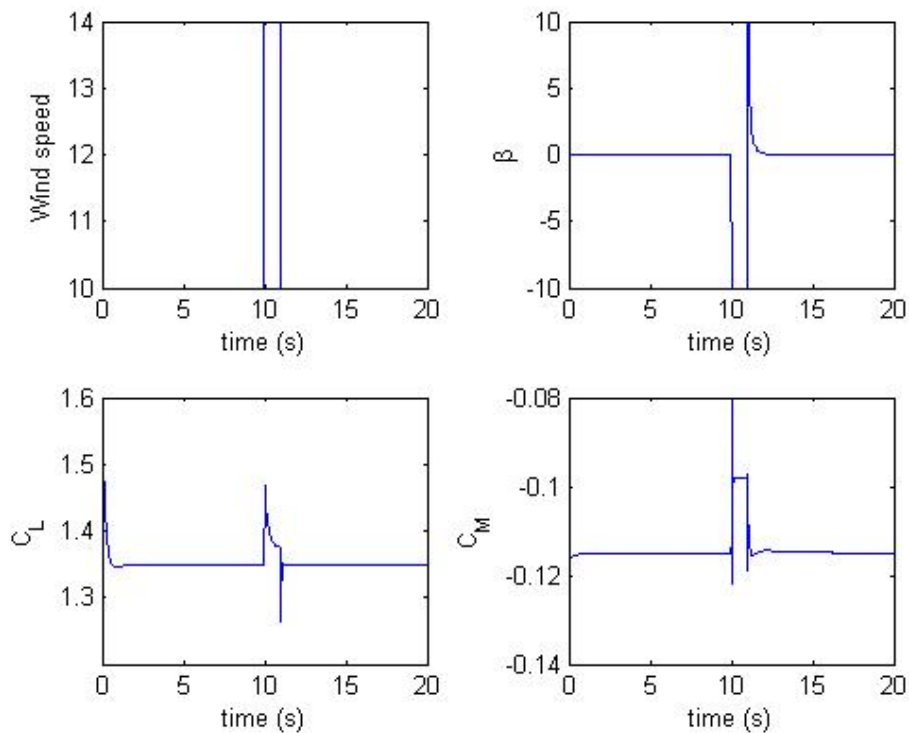


Figure 5 The wind gust is shown in the upper left graph. The active control is seen in the upper right graph. The lower left graph shows  $C_L$  response and the lower right graph shows the  $C_M$  response.

Table 3 Wind gust results. “No con” denotes where the control is inactive, while “Con” denotes where the control is active.

	Std		Mean		Min		Max	
	No con	Con	No con	Con	No con	Con	No con	Con
$C_L$	0.0282	0.0125	1.3552	1.3529	1.2619	1.2652	1.5335	1.4667
$C_D$	0.0170	0.0121	0.0203	0.0189	$-4.17 \cdot 10^{-4}$	-0.0182	0.0936	0.0937
$C_M$	0.0013	0.0041	-0.1145	-0.0803	-0.1149	-0.1218	-0.1091	-0.1137

Table 4 Wind gust results shown in percentage. Increases (shown in negative numbers) and decreases in  $C_L$ ,  $C_D$  and  $C_M$ .

	Diff Std	Diff Mean	Diff Min	Diff Max
$C_L$	55.7%	0.170%	-0.262%	4.36%
$C_D$	28.8%	29.9%	-4261%	-0.107%
$C_M$	-215%	29.9%	-6.01%	-4.22%

### 1.2.3 Turbulent wind

In this section a turbulent wind series is analyzed. The wind series has a mean wind speed of 10m/s with a turbulence intensity of 10%. In Figure 6 the wind series is shown in the upper left plot, while  $C_L$  and  $C_M$  are shown for the case without control in the lower plots. Figure 7 shows the controlled case where the flap deflection is shown in the upper right plot. It is seen that the limit of 10 degrees in flap deflection is reached a few time during the run, however, the flap deflection mainly stays within the range of +/- 5 degrees. In Table 5 the results are given for the case with and without control. In Table 6 the reductions are shown and the reduction in the standard deviation of  $C_L$  is 91.6%. As in the previous cases the standard deviation of  $C_D$  is reduced while the standard deviation of  $C_M$  increases by over 300%.

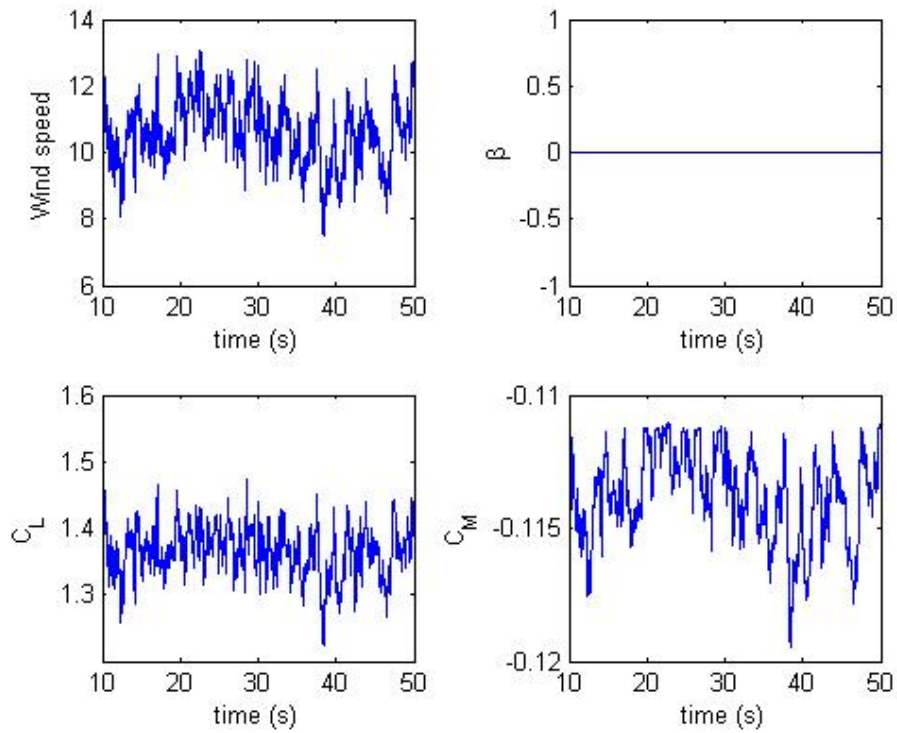


Figure 6 A turbulent wind is shown in the upper left graph. There is no which is seen in the upper right graph. The lower left graph shows  $C_L$  response and the lower right graph shows the  $C_M$  response.

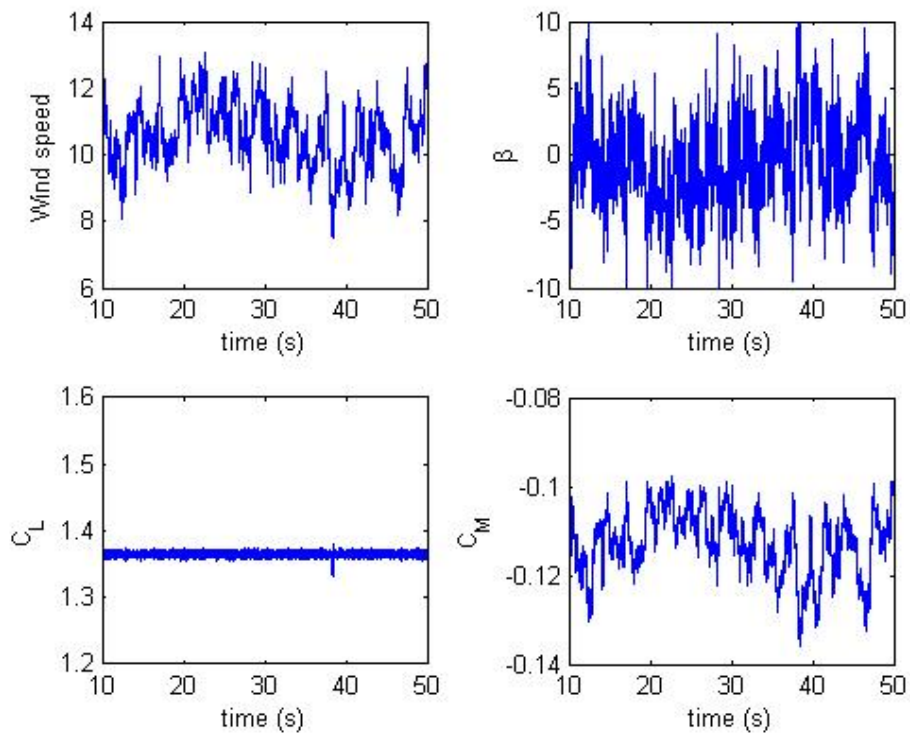


Figure 7 A turbulent wind series is shown in the upper left graph. The active control is seen in the upper right graph. The lower left graph shows  $C_L$  response and the lower right graph shows the  $C_M$  response.

Table 5 Turbulent wind results. “No con” denotes where the control is inactive, while “Con” denotes where the control is active.

	Std		Mean		Min		Max	
	No con	Con	No con	Con	No con	Con	No con	Con
C <sub>L</sub>	0.0359	0.0030	1.3659	1.3649	1.2249	1.3330	1.4740	1.3795
C <sub>D</sub>	0.0126	0.0073	0.0236	0.0187	-0.0038	-0.0044	0.0658	0.0438
C <sub>M</sub>	0.0016	0.0071	-0.1136	-0.1120	-0.1195	-0.1358	-0.1110	-0.0978

Table 6 Turbulent wind results shown in percentage. Increases (shown in negative numbers) and decreases in C<sub>L</sub>, C<sub>D</sub> and C<sub>M</sub>.

	Diff Std	Diff Mean	Diff Min	Diff Max
C <sub>L</sub>	91.6%	0.073%	-8.83%	6.41%
C <sub>D</sub>	42.1%	20.8%	-15.8%	33.4%
C <sub>M</sub>	-342%	1.41%	-13.6%	11.9%

## 2 DUWIND contribution

### 2.1 Description of model

The 1<sup>st</sup> order simulations were carried out using a developed unsteady aerodynamic model for a 2D airfoil with a trailing edge (TE) flap. The modeling is based on thin airfoil theory for a flat airfoil with a flat (rigid) TE flap. The unsteady lift coefficient (Cl), pitching moment coefficient (Cm) and flap hinge moment coefficient (Ch) can be calculated. Since the model is inviscid, the unsteady drag coefficient (Cd) is not calculated, but its viscous quasi-steady values can be used from tabulated data. It is assumed that the flap deflection is not changing considerably the Cd of the airfoil. The camber of the airfoil is taken into account by using the Cl for zero angle of attack and Cl gradient values. The calculations are only valid for small perturbations in the linear region of the Cl-alpha curve. The model is using the indicial theory concept by superimposing the effect of various arbitrary forcing inputs based on their indicial (step) response on the aerodynamic forces and moments (convolution) (see [4] and [5]). It is formulated in state-space form for efficient time integration and controller design. The available arbitrary forcing inputs are: airfoil pitch and plunge motions, TE flap deflection and vertical gust field. The model is pure aerodynamic, so no elastic effects (displacements) from the structure, or flap dynamics have been included.

### 2.2 Description of investigated cases

The 75% radius blade section of the Upwind reference 5MW wind turbine is used. The airfoil is a NACA-64618 with a chord length of 2.8454 m. The pitch axis of the airfoil is located at a length 37%*c* from the leading edge. For all the investigated cases a 10%*c* length TE flap has been used.

The mean wind speed is 10 m/s and the rotational speed of the section is 60 m/s (rotational frequency  $\omega=1.27$  rad/s and radial position  $r=47.25$  m). This makes the resultant velocity at the section  $V_{res}=60.835$  m/s. So, the angle of attack is 9.4595 deg. It must be pointed out that the local twist angle (2.7 degrees) is not taken into account. Also the induced velocities from the turbine wake are also ignored. These two effects would reduce the angle of attack at the section.

The input excitations in wind speed change the resultant velocity and angle of attack at the section. In these simulations, the effect of the gusts and turbulence in wind speed has been simulated by the use of an arbitrary vertical gust field in the model. This makes the simulations more realistic than changing the local angle of attack, since the angle of attack will vary along the airfoil chord during the passage of the varying gust/turbulence, causing an asymmetrical induced upwash.

A feedback controller has been used for the TE flap deflection signal based on the measured values of Cl. The controller is simple PI. Since the current model is always stable and ideal (full knowledge of the system, no delays in controller), no extra effort has been put in the fine-tuning of the controller. The performance of the controller as can be seen in the results is rather high, because of all the simplifications in the system.

## 2.3 Results

### 2.3.1 Wind step

A step in the wind speed:

$$V = \begin{cases} 10 \text{ m/s}, & 0 \text{ s} \leq t < 10 \text{ s} \\ 11 \text{ m/s}, & 10 \text{ s} \leq t \leq 20 \text{ s} \end{cases}$$

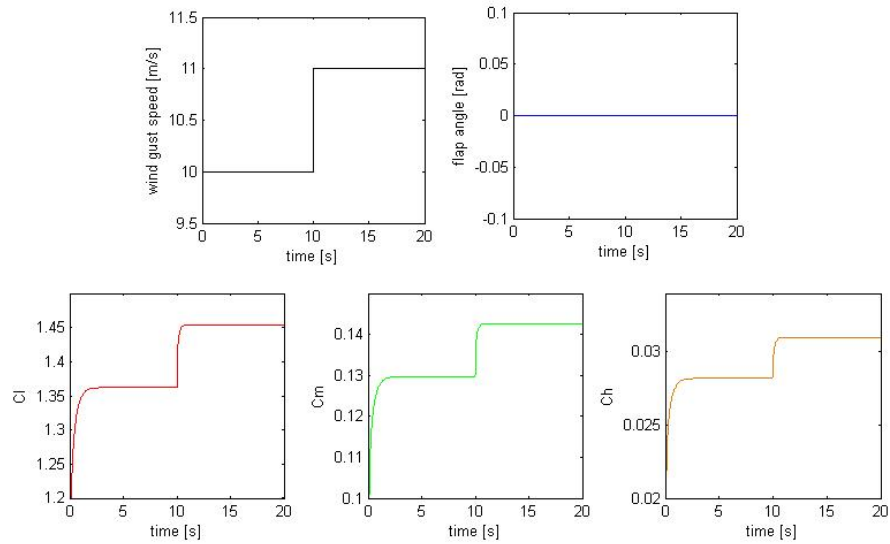


Figure 8 Inputs and response of system for a step in wind speed – No control of TE flap

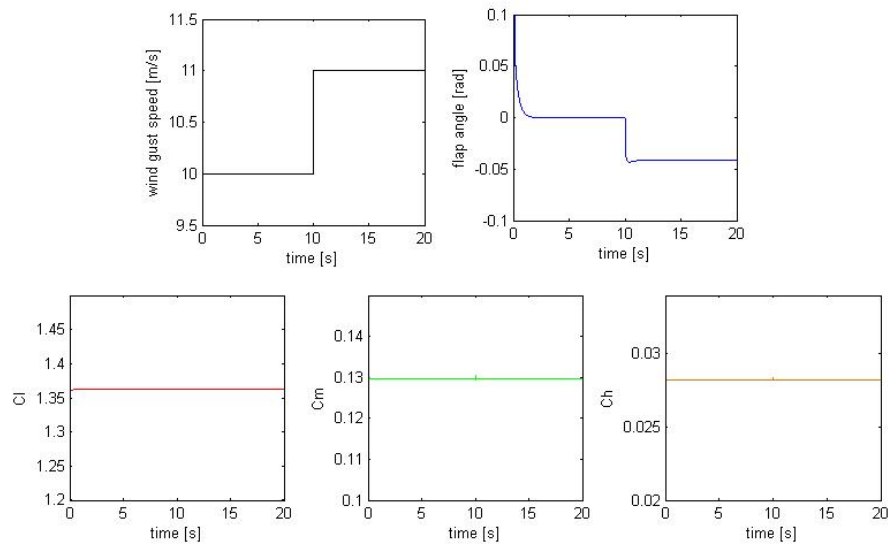


Figure 9 Inputs and response of system for a step in wind speed – Feedback control of TE flap

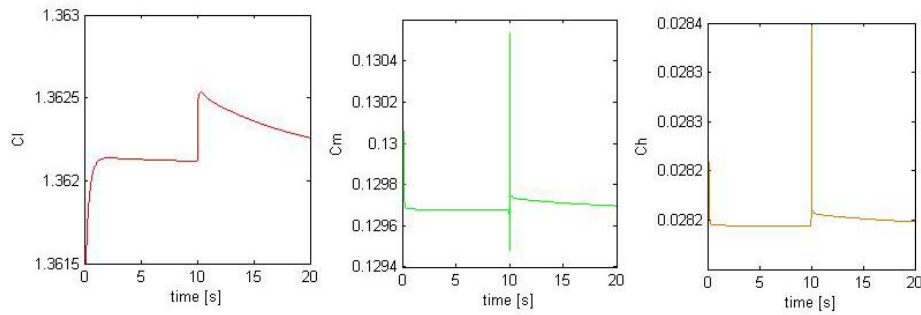


Figure 10 Response of system for a step in wind speed – Feedback control of TE flap (zoom in)

Data analysis:

- Cl range reduction: 99.92%
- Cl peak value reduction: 6.26%
- Cm range reduction: 98.65%
- Cm peak value reduction: 8.49%
- Ch range reduction: 98.8%
- Ch peak value reduction: 8.39%
- Flap angle range: 0.04795 rad
- Maximum flap angle: -0.04782 rad

Comments:

The results show that the peak value of the response due to the sharp wind speed step can significantly be reduced by quick deflection of the TE flap of less than 3 degrees. The control strategy is based on measured Cl, but as a result, the moments variations are also reduced. It should be noted though that the model calculates the moment coefficient around the mid-chord point instead of the quarter-chord point. So, if the values would be transported to the usual 1/4c point, the Cm would probably increase (its negative value). The initial transients and the high instant peaks in the Cm, Ch are due to the numerical model (evaluation of the Kussner function and time calculation of rates in the time integration scheme).

**2.3.2 Square wind input**

A square input (block) in the wind speed:

$$V = \begin{cases} 10m/s, & 0s \leq t < 10s \\ 14m/s, & 10s \leq t \leq 11s \\ 10m/s, & 11s < t \leq 20s \end{cases}$$

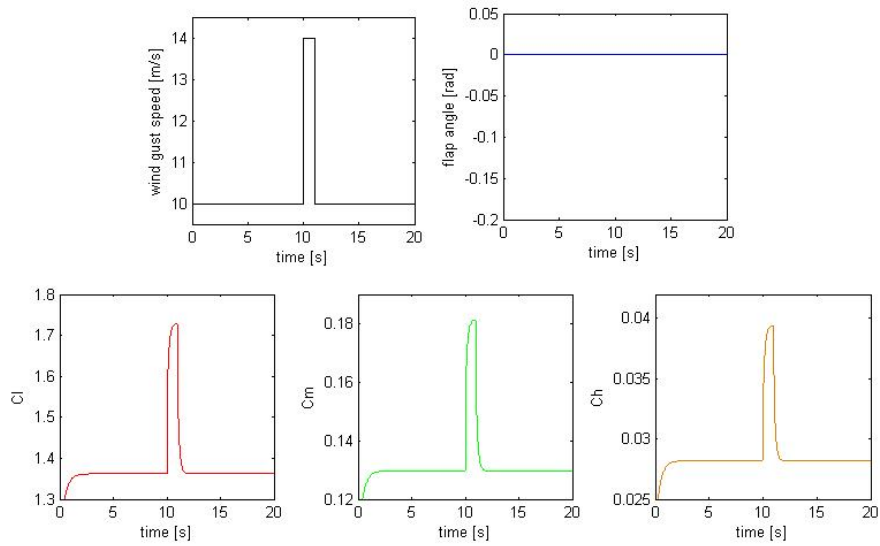


Figure 11 Inputs and response of system for a square wind speed input – No control of TE flap

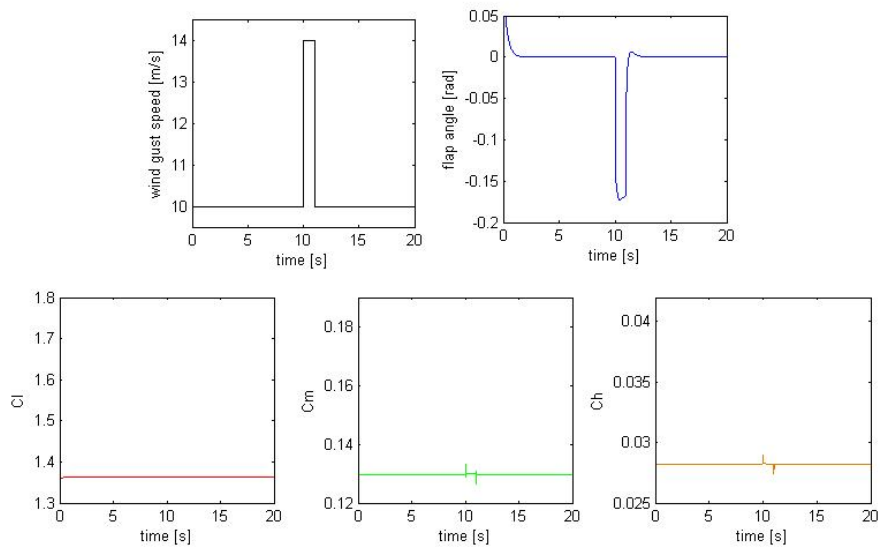
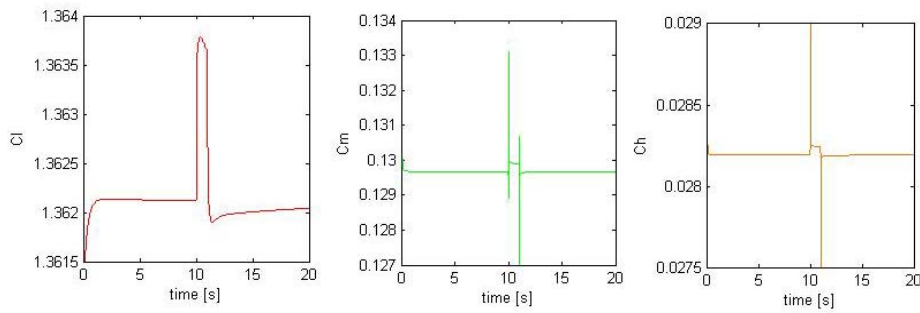


Figure 12 Inputs and response of system for a square wind speed input – Feedback control of TE flap



*Figure 13 Response of system for a square wind speed input – Feedback control of TE flap (zoom in)*

Data analysis:

Cl range reduction: 99.51%  
 Cl peak value reduction: 21.06%  
 Cm range reduction: 87.71%  
 Cm peak value reduction: 26.55%  
 Ch range reduction: 86.59%  
 Ch peak value reduction: 26.37%  
 Flap angle range: 0.1793 rad  
 Maximum flap angle: -0.1727 rad

Comments:

The results show that the peak value of the response due to the fast increase and decrease in wind speed can significantly be reduced by quick deflection of the TE flap. Due to the large increase in the wind speed, the flap deflection is quite big (9.7 deg). No saturation limit on the flap deflection has been implemented. With such a limitation, the peak response would be higher.

**2.3.3 Turbulent wind input**

A turbulent wind input with 10% turbulence intensity.

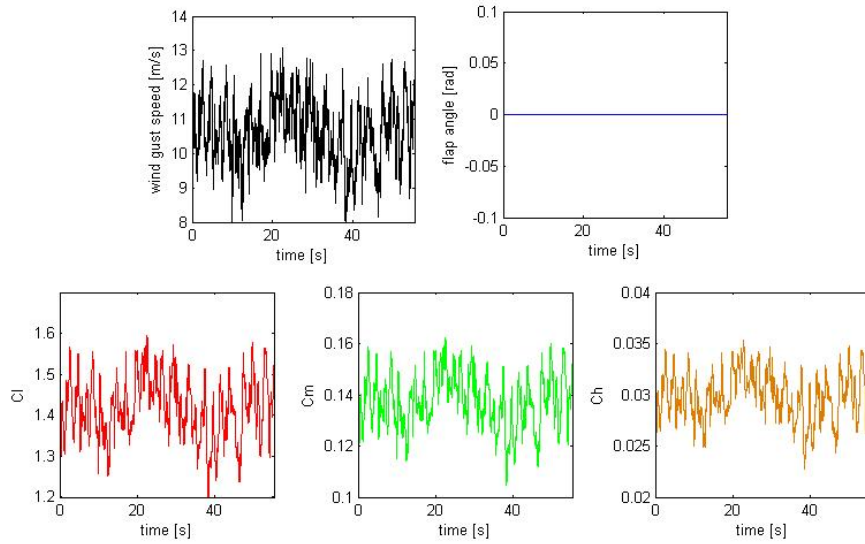


Figure 14 Inputs and response of system for a turbulent wind speed input – No control of TE flap

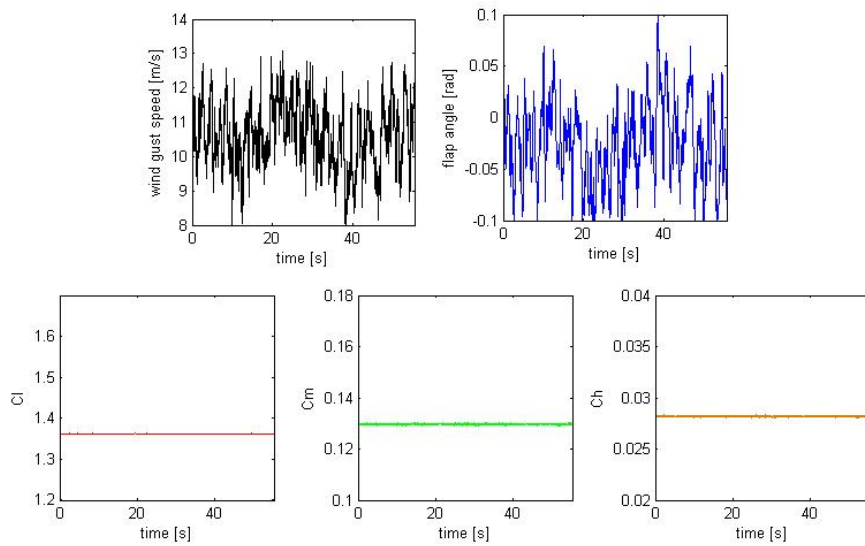


Figure 15 Inputs and response of system for a turbulent wind speed input – Feedback control of TE flap

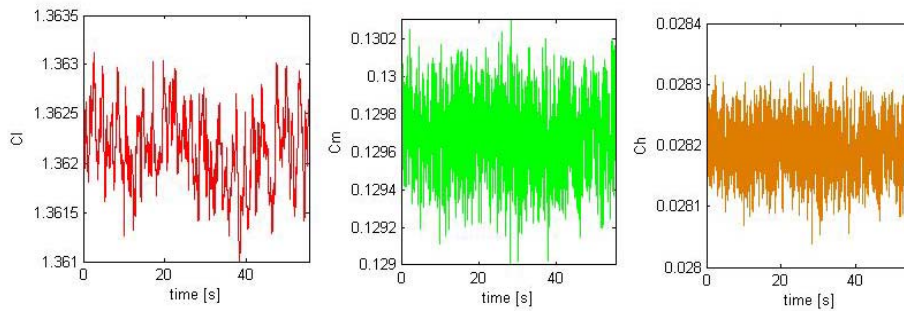


Figure 16 Response of system for a turbulent wind speed input – Feedback control of TE flap (zoom in).

Data analysis:

- Cl range reduction: 99.45%
- Cl std reduction: 99.5%
- Cm range reduction: 97.73%
- Cm std reduction: 98.42%
- Ch range reduction: 97.68%
- Ch std reduction: 98.61%
- Flap angle range: 0.2138 rad
- Maximum flap angle: -0.1154 rad

Comments:

The results show that the range of fluctuations of the response due to the turbulent wind speed can significantly be reduced by using the TE flap with deflections less than 7 deg.

### 3 Conclusion.

Two codes have been tested on identical airfoils and in three cases, in order to evaluate the performance of trailing edge flaps on the reduction of unsteady loads in a 2D test case. There are several differences in the two models, which also can be seen in the results. Generally, the reduction of varying  $C_L$  is large. In the wind step case both models agree on larger than 90% reduction, however, the Risø model does not reduce as much as the Delft model for the “wind gust” case. This is mainly due to the Risø model is including stall and that there is imposed a limit on the flap angle deflection of 10 degrees. The effect of this saturation limit on the flap can also be seen in the turbulent wind case. The instantaneous big jumps of wind speed (especially in the “wind gust” case) lead to angles of attack above the static maximum value, so the use of a dynamic stall model produces more conservative results regarding the Cl reduction, compared to the attached flow one. Also, the flexibility of the TE camber (compared to the rigid flap) has a slight effect on the Cl response due to the flap deflection which must be taken into consideration. The difference on the Cm response between the two models must be pointed out, since the Delft model calculates the pitching moment response on the mid-chord point instead of the 1/4c one, so the large negative response like in the model of Risø cannot be seen. Generally, both approaches show the potential in controlling the fluctuations of local aerodynamic forces on wind turbine blade sections using trailing edge flaps. Although the modeling includes certain assumptions, the great load alleviation potential is shown. Further investigations will extend the research on more elaborate modeling.

## 4 References

- [1] Gaunaa, M., “Unsteady 2D Potential-flow Forces on a Thin Variable Geometry Airfoil Undergoing Arbitrary Motion”, Risø-R-1478, Risø, Roskilde, Denmark, June 2004.
- [2] Hansen, M.H., Gaunaa, M., Madsen, H.Aa. “A Beddoes-Leishman type dynamic stall model in state-space and indicial formulations”, Risø-R-1354, Risø, Roskilde, Denmark, June 2004.
- [3] von Karman, Th. & Sears, W.R., “Airfoil Theory for Non-Uniform Motion.”, *Journal of the Aerodynamical Science*. 5(10) 1938. p.379-390.
- [4] Leishman, J.G., “Unsteady lift of a flapped airfoil by indicial concepts”, *Journal of Aircraft*, Vol. 31, No. 2, 1994.
- [5] Leishman, J.G., “Principles of Helicopter Aerodynamics”, 2<sup>nd</sup> edition, 2005.

Risø's research is aimed at solving concrete problems in the society.

Research targets are set through continuous dialogue with business, the political system and researchers.

The effects of our research are sustainable energy supply and new technology for the health sector.

